AGU PUBLICATIONS

Geophysical Research Letters

RESEARCH LETTER
10.1002/2015GL066703

Key Points:
- Mesospheric effects of NO_x enhancements due to energetic particle precipitation (EPP) are modeled
- NO_x enhancement leads to HO_x repartitioning which increases ozone loss by catalytic HO_x reactions
- Energetic particle precipitation could have a longer-term, wintertime effect on mesospheric ozone

Correspondence to:
P. T. Verronen,
pekka.verronen@fmi.fi

Citation:
Verronen, P. T., and R. Lehmann (2015), Enhancement of odd nitrogen modifies mesospheric ozone chemistry during polar winter, *Geophys. Res. Lett.*, *42*, 10,445–10,452, doi:10.1002/2015GL066703.

Received 23 OCT 2015
Accepted 16 NOV 2015
Accepted article online 24 NOV 2015
Published online 8 DEC 2015

Enhancement of odd nitrogen modifies mesospheric ozone chemistry during polar winter

P. T. Verronen[1] and R. Lehmann[2]

[1]Earth Observation Unit, Finnish Meteorological Institute, Helsinki, Finland, [2]Alfred Wegener Institute for Polar and Marine Research, Potsdam, Germany

Abstract Energetic particle precipitation (EPP) enhances odd nitrogen (NO_x) in the polar upper atmosphere. Model studies have reported a solar cycle response in mesospheric ozone (O_3) caused by EPP-related NO_x enhancements which are included by applying a vertical NO_x flux at around 80 km. However, it is not clear how O_3 can be affected when the main chemical catalyst of odd oxygen ($O_x = O + O(^1D) + O_3$) loss in the mesosphere is odd hydrogen (HO_x). Here we use a 1-D atmospheric model and show how enhanced NO_x affects mesospheric chemistry and changes HO_x partitioning, which subsequently leads to increase in O_x loss through standard HO_x-driven catalytic cycles. Another, smaller increase of O_x loss results from HO_x storage in HNO_3 during night and its release by daytime photodissociation. Our results suggest that EPP, through NO_x enhancements, could have a longer-term effect on mesospheric HO_x and O_x in polar winter.

1. Introduction

Energetic particle precipitation (EPP) affects the neutral chemistry of the polar middle atmosphere [*Sinnhuber et al.*, 2012; *Verronen and Lehmann*, 2013]. For example, EPP leads to production of odd hydrogen ($HO_x = H + OH + HO_2$) and odd nitrogen ($NO_x = N + NO + NO_2$) through impact ionization, dissociation and ion chemistry, and subsequently to ozone depletion through well-known catalytic reaction sequences. Over the solar cycle, there is evidence of EPP causing mesospheric ozone variation by tens of percent, with possible dynamical connections to ground level regional climate variability [*Andersson et al.*, 2014, and references therein].

During EPP events, HO_x is the main driver of mesospheric ozone changes and causes up to 90% depletion during large solar proton events (SPE) [*Verronen et al.*, 2006]. HO_x production by EPP occurs only below about 80 km altitude where enough water vapor is available. At these altitudes, the chemical lifetime of HO_x is relatively short (days), the EPP effects are short term, and mesospheric ozone typically recovers in a few days after an event [e.g., *Funke and et al.*, 2011; *Jackman et al.*, 2014].

EPP NO_x is produced continuously in the high-latitude lower thermosphere by auroral electrons [*Barth*, 1992]. In wintertime, when the NO_x chemical lifetime is long (months), large amounts of NO_x can gradually descent to mesospheric and stratospheric altitudes inside the polar vortex [e.g., *Randall et al.*, 2009; *Funke et al.*, 2014]. In the mesosphere, NO_x can be enhanced tenfold over the winter months due to descent from altitudes above, complemented by in situ production during strong EPP events (e.g., SPE) [*Seppälä et al.*, 2007].

When modeling the atmospheric effects, typically both HO_x and NO_x production is parameterized and scaled with altitude-dependent EPP ionization rates [e.g., *Funke and et al.*, 2011, and references therein]. However, to account for the production of NO_x by auroral electrons, models that do not cover the lower thermosphere are restricted to using an upper boundary condition (NO_x-UBC), e.g. by applying a vertical NO_x flux at around 80 km [*Baumgaertner et al.*, 2011]. NO_x-UBC allows for studies of NO_x descent from the model top toward the stratosphere [e.g., *Salmi et al.*, 2011], but it neglects EPP-related HO_x production occurring below the model top.

In the mesosphere, the odd oxygen ($O_x = O + O(^1D) + O_3$) loss due to the catalytic NO_x cycles is orders of magnitude smaller than the loss due to the HO_x cycles [e.g., *Grenfell et al.*, 2006]. Despite this, some model studies have suggested that NO_x increase leads to mesospheric ozone response on solar cycle time scales at wintertime polar latitudes. *Baumgaertner et al.* [2011] used a NO_x-UBC method to study the effect of auroral electrons, and showed up to 0.5 ppmv decrease in ozone at 70–80 km. The reasons behind the mesospheric

response were not discussed, but they seem to be related to the NO_x increase caused by the NO_x-UBC. *Rozanov et al.* [2012] used a combination of EPP forcing: ionization-driven HO_x and NO_x production for solar proton events within the model altitude range and NO_x-UBC at about 80 km for auroral electrons (the same method as in *Baumgaertner et al.* [2011]). They reported decrease in ozone at 70–80 km, reaching to about 10%. Although it is possible that some of the ozone response was due to SPE HO_x, they noted that the ozone depletion in the mesosphere (and the stratosphere) followed the time evolution of the NO_x enhancement. Thus, part of the mesospheric ozone response could have been caused by the enhanced NO_x.

Other studies, using models with ionization-driven EPP NO_x and HO_x production, have also indicated solar cycle or longer-term responses in mesospheric ozone in polar winter. However, these studies did not discuss or mention any NO_x contribution to ozone response, although increases in NO_x were also reported. *Marsh et al.* [2007] presented ≈10% decrease in ozone around 80 km in response to solar cycle variability in irradiance and auroral electron precipitation, the effect being caused by changes in photolysis of H_2O by Lyman-alpha radiation (which is a source of HO_x). Also, *Jackman et al.* [2009] showed about 5% decrease in yearly averaged mesospheric ozone at 70–80 km due to SPEs, and the ozone response was mainly caused by the large HO_x increases occurring during the events. Similarly, *Semeniuk et al.* [2011] found a large (up to several tens of percent) EPP-related solar cycle response in ozone at 60–80 km, caused by enhanced catalytic HO_x cycles.

In summary, it seems that NO_x has an impact on mesospheric ozone in models which describe (at least part of) the EPP forcing with NO_x-UBC (and thus neglect the HO_x production). On the other hand, models that include ionization-driven NO_x and HO_x production seem to agree that HO_x is the main driver of ozone changes. Mechanisms that could connect NO_x enhancements to significant ozone loss are unclear.

In this paper, we use a 1-D atmospheric model to study the connection between NO_x enhancements and O_x (and thus ozone) depletion in the mesosphere. Our aim is to provide a detailed analysis of chemical mechanisms that can lead to an O_x response in the presence of large NO_x amounts. We are going to demonstrate that the catalytic NO_x cycles alone are not significant but modification of the HO_x chemistry by an enhanced NO_x concentration can produce a noticeable effect.

2. Modeling

The Sodankylä Ion and Neutral Chemistry (SIC) is a 1-D atmospheric model which solves for concentrations of 16 neutral and 72 ionic species at altitudes between 20 and 150 km, taking into account about 400 ion-neutral reactions, and molecular and eddy diffusion. A detailed description of the model is given elsewhere [e.g., *Verronen et al.*, 2005]. For mesospheric neutral chemistry of NO_x, HO_x, and O_x species, SIC includes the standard set of reactions and rate coefficients from *Sander et al.* [2006].

In our study, we proceeded as follows. First, SIC was initialized for July conditions at 72.0°S, 2.5°E (the Troll station in Antarctica, in wintertime). Second, we made two model runs for the time period between 20 and 25 July 2009: a "normal" control run (from now on the "CTR" run) and a run with a manually imposed, somewhat arbitrary enhancement of NO_x initial concentrations in the mesosphere (the "ENOX" run). The applied enhancement (see Figure 1) is realistic, however, and comparable, e.g., to the wintertime year-to-year variability observed at high latitudes [*Funke et al.*, 2014, Figure 10]. Note that our conclusions on the mechanisms of mesospheric chemistry response, as presented in the following sections, are not so much dependent on the magnitude of the applied NO_x enhancement, although the magnitude of the response obviously is.

For the selected location and solar illumination conditions (note that other similar settings could have been selected as well), the NO_x chemical lifetime is long (about half a year at 75 km) and a large fraction of the enhanced initial concentration will survive throughout the modeling period, allowing us to study the effects on O_x chemistry during this time.

In our analysis, we mainly use reaction rate plots as indication of changes in model chemistry. In addition, in order to obtain complete catalytic O_x loss cycles and their rates, we apply the reaction pathway analysis algorithm by *Lehmann* [2004].

We emphasize that we are comparing two scenarios, one characterized by low NO_x and another by high NO_x, which could be generated by low- and high-EPP forcing. But we are not fully reproducing the effects of EPP because we are (intentionally) neglecting all other impacts, for example, HO_x production [*Verronen et al.*, 2006], which means that our results as such cannot be confirmed by observations. Also, temperature and

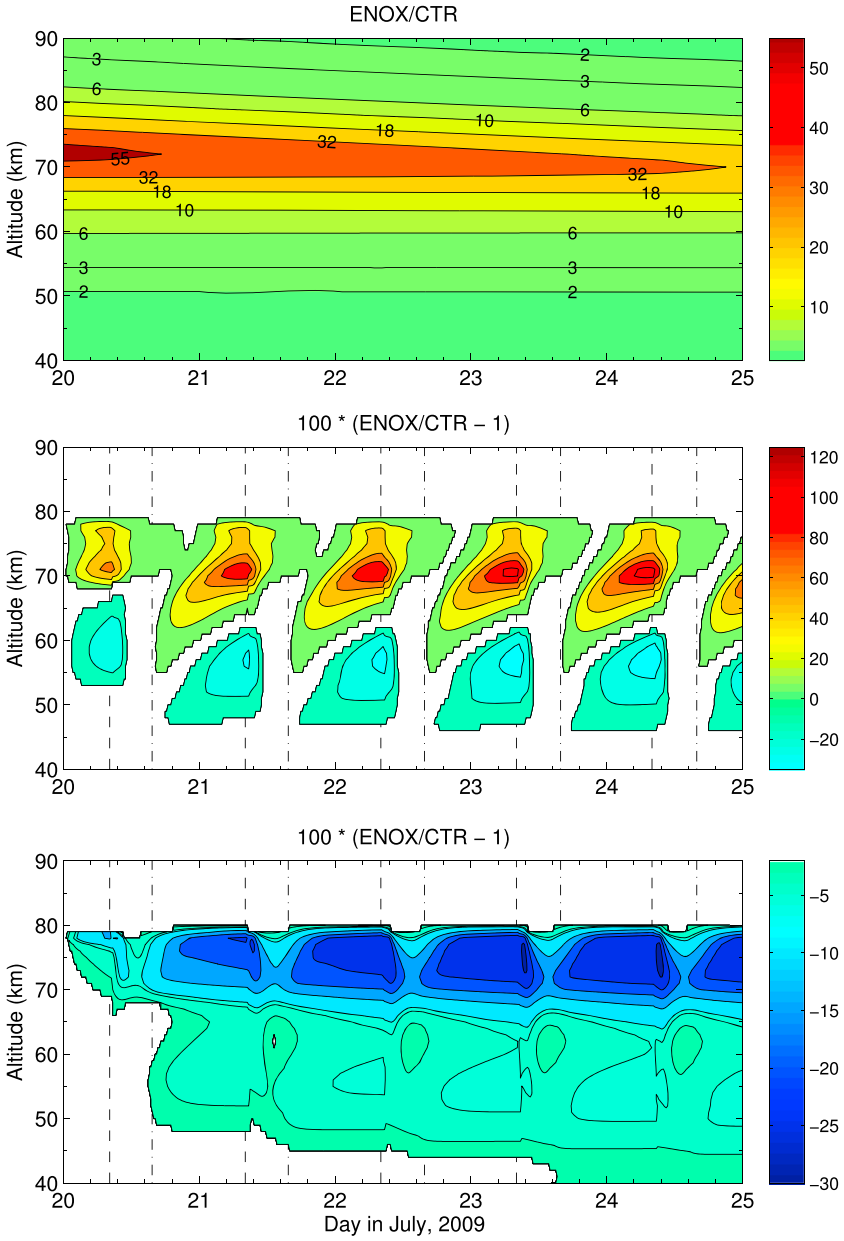

Figure 1. Relative difference between ENOX and CTR model runs. (top) NO_x, (middle) HO_x, and (bottom) O_x. The white areas in middle and bottom panels indicate ENOX-CTR difference within ±5% and ±1%, respectively. The vertical dash and dash-dotted lines indicate sunrise and sunset times (solar zenith angle = 100°), respectively.

other dynamical effects taking place in wintertime mesosphere (e.g., horizontal mixing and/or air descent) can have an impact on HO_x and O_x [*Smith et al.*, 2009; *Damiani et al.*, 2010], which is not taken into account in our analysis. Nevertheless, as shown in the following section, our approach is useful in understanding the chemical mechanisms leading from NO_x increase to O_x loss.

3. Results and Discussion

Figure 1 shows the relative difference in NO_x, HO_x, and O_x concentrations between the ENOX and CTR model runs. As discussed in section 2, the NO_x initial concentrations were manually enhanced for the ENOX run. In the beginning of the modeling period, the applied increase varies from a factor of 1 (no increase) at 40 km to about a factor of 60 at 72 km before decreasing to a factor of about 2 at 90 km. As the modeling advances in time, NO_x recovers above 65 km toward lower values due to both chemistry and dynamics (vertical diffusion).

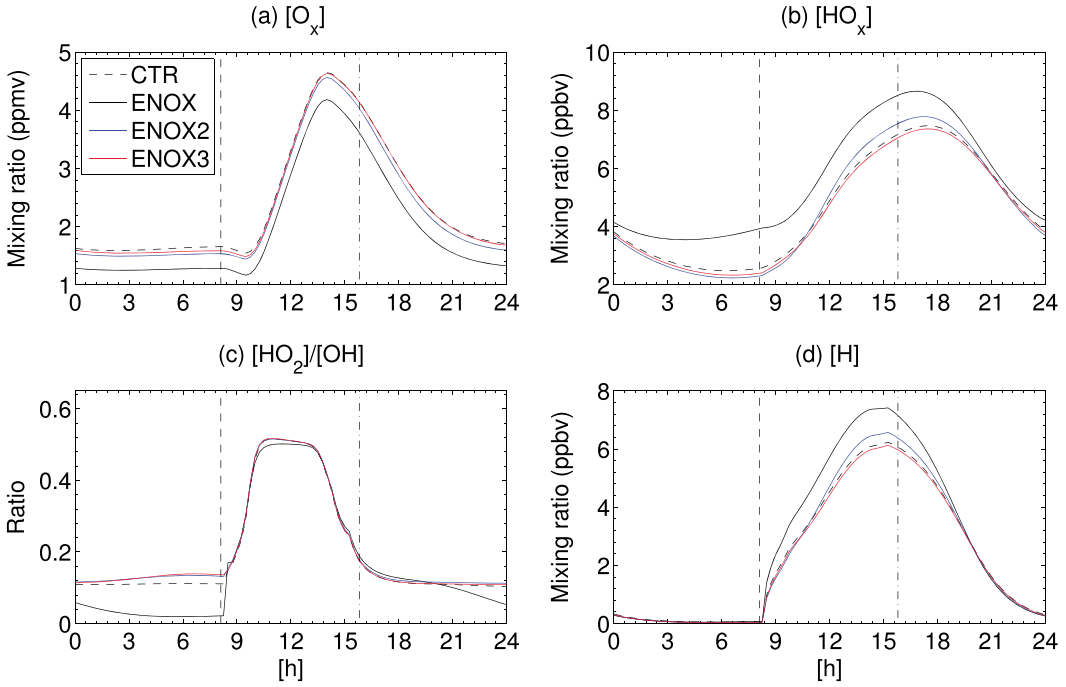

Figure 2. (a) O_x mixing ratio on 22 July at 75 km from the CTR, ENOX (with reactions R052 and R053 included), ENOX2 (with R053, without R052), and ENOX3 (without R052 and R053) model runs. The vertical dash and dash-dotted lines indicate sunrise and sunset times (solar zenith angle = 100°), respectively. (b) Mixing ratio of HO_x. (c) Ratio $[HO_2]/[OH]$. (d) Mixing ratio of H.

However, this decrease is relatively slow because the loss of NO_x through photodissociation ($NO + h\nu \rightarrow N + O$ followed by $N + NO \rightarrow N_2 + O$) is moderate in the near polar night conditions. Below 65 km, the loss of NO_x is not significant and the enhanced values survive throughout the modeling period.

O_x concentrations are significantly decreased when the chemical system has adapted to the NO_x increase after one diurnal cycle. As $[O_3]/[O_x]$ is almost the same in both runs, Figure 1 would be nearly identical if O_3 was plotted instead of O_x. At 70–80 km, O_x values are persistently lower by 15–30% and 5–15% at nighttime and daytime, respectively. Note that the absolute change is about the same at day and night, e.g., on 22 July as shown in Figure 2a. The day/night difference in relative change is caused by the diurnal cycle of O_x (maximum in the afternoon). Another region of O_x change is seen at 55–65 km where the values are 2–5% lower. Later on, the affected altitude region extends down to 40 km.

Also HO_x concentrations are affected, and again the changes are persistent after one diurnal cycle. Increases are seen between 65 and 80 km, ranging between 5 and 100%, with maximum enhancement at 70 km. The absolute difference of HO_x between CTR and ENOX increases during late night, is nearly constant during daytime, and decays after sunset (Figure 2b). On the other hand, the HO_x mixing ratio increases during daytime and decreases after sunset. These diurnal variations lead to the maximum of the relative difference around sunrise as seen in Figure 1. Except between sunset and midnight, when the enhancements extend down to 55 km, there is an altitude region of HO_x decrease at 45–60 km where the values are lower by 5–30%. Maximum decrease is seen at about 55 km.

From Figure 1 it is already quite evident that the O_x decrease below 60 km is likely caused directly by the NO_x increase, because the HO_x decrease seen at these altitudes would imply an O_x increase. This is confirmed by our pathway analysis: although at 55 km the main catalytic loss cycles are HO_x-dependent, the NO_x-driven cycles are also significant, and the decrease in O_x is caused by the increase in NO_x-driven catalytic loss. For example, at 55 km the NO_x cycles are causing 6% of O_x loss in CTR and 18% in ENOX on 22 July (averaged over 24 h).

Above 65 km, understanding the O_x decrease is not as straightforward because the NO_x increase results also in HO_x increase. Figure 3 shows that at 75 km, despite the high NO_x concentration, the O_x loss is clearly

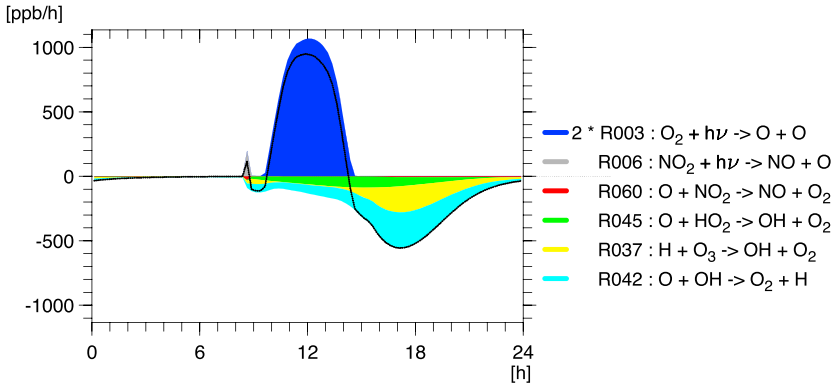

Figure 3. Most important production and loss reactions of O_x (= O + O(^{1}D) + O_3) on 22 July at 75 km (ENOX run). The black line indicates net rate of change.

dominated by HO_x reactions. All the loss reactions in Figure 3 are part of catalytic O_x loss cycles according to the pathway analysis. The reaction

$$H + O_2 + M \rightarrow HO_2 + M \text{ (R035)}$$

closes the cycle containing the reactions

$$O + HO_2 \rightarrow OH + O_2 \text{ (R045)}$$

and

$$O + OH \rightarrow O_2 + H \text{ (R042)}.$$

The contribution of NO_x reactions is small. For example, at 75 km the integrated (over 24 h) rate of the NO_x cycles is less than 5% of the total O_x loss in the ENOX run. However, we find that the NO_x increase does

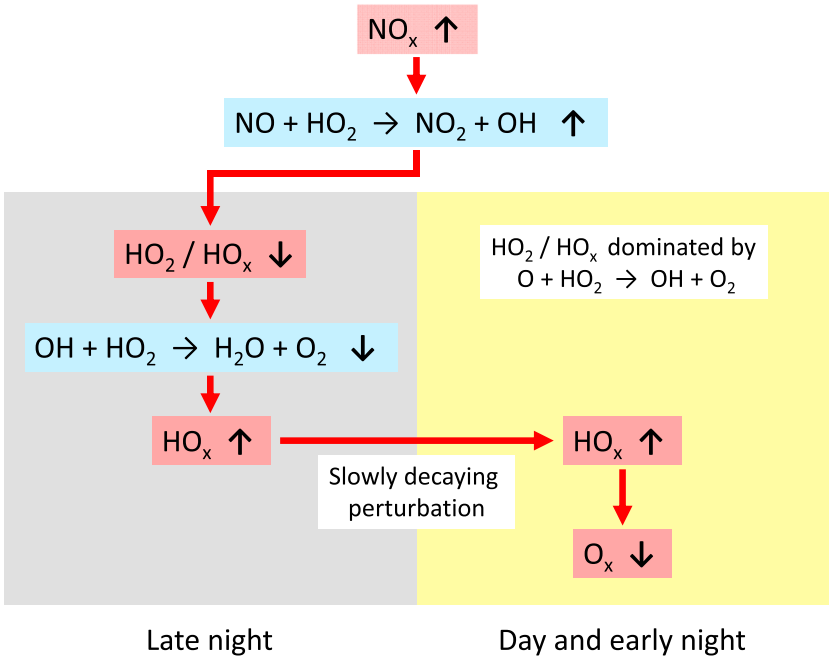

Figure 4. Schematic view of NO_x enhancements leading to HO_x and O_x changes. Red arrows indicate the sequence of effects, black arrows indicate increase (up) or decrease (down) of reaction rates, HO_x partitioning, or gas concentrations.

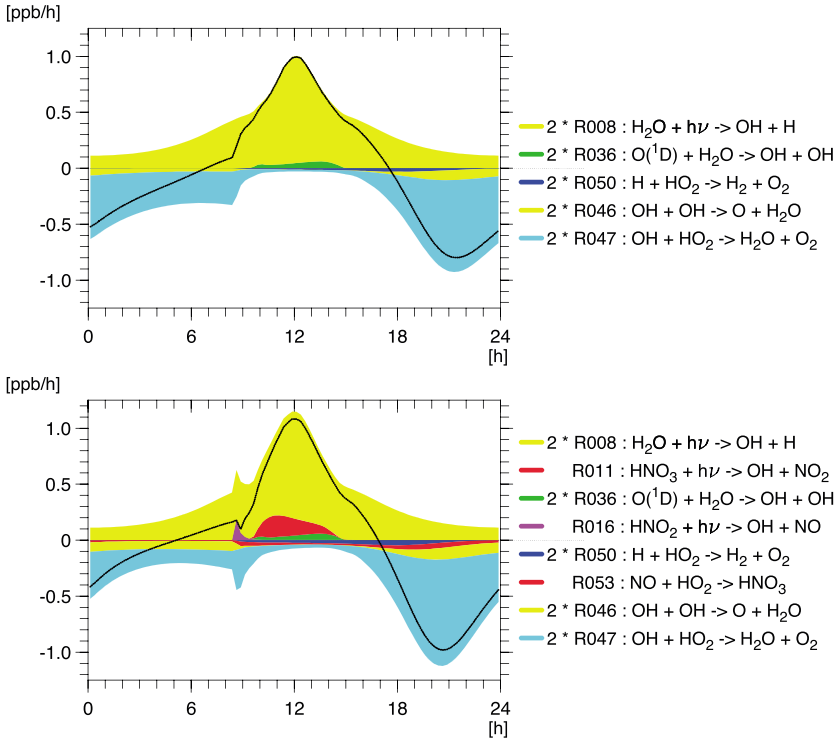

Figure 5. Most important production and loss reactions of HO_x (= H + OH + HO_2) on 22 July at 75 km. (top) CTR run, (bottom) ENOX run. The black line indicates net rate of change.

affect O_x, indirectly, through changing HO_x partitioning and loss as demonstrated schematically in Figure 4. The reaction

$$NO + HO_2 \rightarrow NO_2 + OH \text{ (R052)}$$

is significantly enhanced which leads to a smaller $[HO_2]/[OH]$ ratio at night (Figure 2c). As $[OH] \approx [HO_x]$ in both runs, it follows that $[OH] \times [HO_2]$ is smaller in the ENOX run. Consequently, the rate of

$$OH + HO_2 \rightarrow H_2O + O_2 \text{ (R047)}$$

is smaller (at 3:00 approximately half of the rate in the CTR run, Figure 5), leading to less HO_x loss during night and a larger amount of HO_x at the end of the night (cf. Figures 1 and 2b). A large part of the nighttime HO_x increase survives through the day due to its chemical lifetime (several days at daytime, in near polar night conditions) and has a decreasing effect on O_x as explained in more detail in the following.

The HO_x lifetime is longer during the day because most HO_x is converted into H by R042 (Figure 2d). That is why the rates of the HO_x loss reactions R047 and $OH + OH \rightarrow O + H_2O$ (R046) decrease significantly (cf. Figure 5). The longer lifetime of HO_x and the O_x loss are related during daytime, because they both involve atomic oxygen.

Contrary to the night, during daytime the HO_x partitioning is dominated by reactions involving O and H: R042, $H + O_3 \rightarrow OH + O_2$ (R037), R035, and R045. Consequently, the HO_x partitioning is not influenced by the increased NO_x (in the ENOX run) during daytime, so that [H], [OH], and $[HO_2]$ increase (from CTR to ENOX) proportionally to $[HO_x]$ (Figures 2b–2d), leading to more O_x loss (cf. reactions in Figure 3).

At 55 km, the effect of HO_x repartitioning is contrary to that above 65 km (Figure 1). The decrease of the $[HO_2]/[OH]$ ratio through R052 leads to HO_x decrease rather than increase, because at 55 km the dominant HO_x species during night is HO_2.

There is also a second indirect NO_x effect on O_x at 75 km, through temporary storage of HO_x in HNO_3 (and to a lesser extent in HNO_2). The increase of NO_x enhances

$$NO + HO_2 \rightarrow HNO_3 \text{ (R053)}$$

and thus protects some HO_x against loss during night, because it is stored temporally in HNO_3 and will be released through HNO_3 photolysis during the subsequent day (Figure 5, ENOX run). This mechanism increases HO_x concentration and thus O_x loss during daytime. The HO_x storage effect is somewhat similar to what has been reported to take place in the lower mesosphere during solar proton events [*Verronen et al.*, 2006].

To confirm the role of R052 and R053 in the NO_x-induced O_x changes, we repeated the ENOX run twice: first, after removing R052 from SIC ("ENOX2"), and then after removing both R052 and R053 ("ENOX3"). The resulting HO_x and O_x mixing ratios at 75 km are presented in Figure 2, together with those from the CTR and ENOX runs. Note that the NO_x values are practically the same in the ENOX, ENOX2, and ENOX3 runs (not shown). Clearly, R052 removal also removes most of the HO_x and O_x impact. Therefore, we can conclude that the HO_x repartitioning through R052 is the dominant factor and causes most of the O_x difference between the CTR and ENOX runs at 75 km. Also, the HO_x storage through R053 is affecting the HO_x and O_x chemistry, as seen by comparing ENOX2 and ENOX3, although the effect is smaller than the HO_x repartitioning effect. The effect of the enhanced NO_x on O_x without HO_x repartitioning and storage, but including the increased rates of the catalytic NO_x cycles, is indicated by the difference between the CTR and ENOX3 runs (Figure 2a). The effect is negligible except at late night and sunrise when it is still only a small fraction of the combined effect of R052 and R053.

4. Summary

Here we have demonstrated theoretically that NO_x increase can, through HO_x repartitioning or temporary storage and resulting decrease of HO_x loss, lead to depletion of mesospheric O_x. This finding is significant because it suggests a persistent, long-term (lasting months) EPP O_x effect in the mesosphere in wintertime when NO_x chemical lifetime is long. Further, it is likely that the HO_x repartitioning by NO_x is causing the solar cycle response in mesospheric ozone which has been reported in some previous modeling studies imposing EPP-related NO_x enhancements [*Baumgaertner et al.*, 2011; *Rozanov et al.*, 2012]. Thus, the NO_x effect may be an important addition to the EPP HO_x impact from which, on an event-by-event basis, mesospheric ozone typically recovers in days after the EPP forcing stops [*Andersson et al.*, 2014]. Specifically, at least part of the long-term response in other models, reported to be HO_x-driven [*Jackman et al.*, 2009; *Semeniuk et al.*, 2011], could be in fact caused by enhanced NO_x prolonging the mesospheric ozone depletion through HO_x.

Acknowledgments
P.T.V. was supported by the Academy of Finland project 276926 (SECTIC: Sun-Earth Connection Through Ion Chemistry). Data used in this study are available upon request from the corresponding author.

References

Andersson, M. E., P. T. Verronen, C. J. Rodger, M. A. Clilverd, and A. Seppälä (2014), Missing driver in the Sun-Earth connection from energetic electron precipitation impacts mesospheric ozone, *Nature Commun.*, *5*(5197), doi:10.1038/ncomms6197.

Barth, C. A. (1992), Nitric oxide in the lower thermosphere, *Planet. Space Sci.*, *40*, 315–336.

Baumgaertner, A. J. G., A. Seppälä, P. Jöckel, and M. A. Clilverd (2011), Geomagnetic activity related NO_x enhancements and polar surface air temperature variability in a chemistry climate model: Modulation of the NAM index, *Atmos. Chem. Phys.*, *11*, 4521–4531, doi:10.5194/acp-11-4521-2011.

Damiani, A., M. Storini, M. L. Santee, and S. Wang (2010), Variability of the nighttime OH layer and mesospheric ozone at high latitudes during northern winter: Influence of meteorology, *Atmos. Chem. Phys.*, *10*, 10,291–10,303, doi:10.5194/acp-10-10291-2010.

Funke, B., et al. (2011), Composition changes after the "Halloween" solar proton event: The high-energy particle precipitation in the atmosphere (HEPPA) model versus MIPAS data intercomparison study, *Atmos. Chem. Phys.*, *11*, 9089–9139, doi:10.5194/acp-11-9089-2011.

Funke, B., M. López-Puertas, G. P. Stiller, and T. von Clarmann (2014), Mesospheric and stratospheric NO_y produced by energetic particle precipitation during 2002–2012, *J. Geophys. Res. Atmos.*, *119*, 4429–4446, doi:10.1002/2013JD021404.

Grenfell, J. L., R. Lehmann, P. Mieth, U. Langematz, and B. Steil (2006), Chemical reaction pathways affecting stratospheric and mesospheric ozone, *J. Geophys. Res.*, *111*, D17311, doi:10.1029/2004JD005713.

Jackman, C. H., D. R. Marsh, F. M. Vitt, R. R. Garcia, C. E. Randall, E. L. Fleming, and S. M. Frith (2009), Long-term middle atmospheric influence of very large solar proton events, *J. Geophys. Res.*, *114*, D11304, doi:10.1029/2008JD011415.

Jackman, C. H., C. E. Randall, V. L. Harvey, S. Wang, E. L. Fleming, M. López-Puertas, B. Funke, and P. F. Bernath (2014), Middle atmospheric changes caused by the January and March 2012 solar proton events, *Atmos. Chem. Phys.*, *14*, 1025–1038, doi:10.5194/acp-14-1025-2014.

Lehmann, R. (2004), An algorithm for the determination of all significant pathways in chemical reaction systems, *J. Atmos. Chem.*, *47*, 45–78.

Marsh, D. R., R. R. Garcia, D. E. Kinnison, B. A. Boville, F. Sassi, S. C. Solomon, and K. Matthes (2007), Modeling the whole atmosphere response to solar cycle changes in radiative and geomagnetic forcing, *J. Geophys. Res.*, *112*, D23306, doi:10.1029/2006JD008306.

Randall, C. E., V. L. Harvey, D. E. Siskind, J. France, P. F. Bernath, C. D. Boone, and K. A. Walker (2009), NO_x descent in the Arctic middle atmosphere in early 2009, *Geophys. Res. Lett.*, *36*, L18811, doi:10.1029/2009GL039706.

Rozanov, E., M. Calisto, T. Egorova, T. Peter, and W. Schmutz (2012), The influence of precipitating energetic particles on atmospheric chemistry and climate, *Surv. Geophys.*, *33*, 483–501, doi:10.1007/s10712-012-9192-0.

Salmi, S.-M., P. T. Verronen, L. Thölix, E. Kyrölä, L. Backman, A. Y. Karpechko, and A. Seppälä (2011), Mesosphere-to-stratosphere descent of odd nitrogen in February–March 2009 after sudden stratospheric warming, *Atmos. Chem. Phys.*, *11*, 4645–4655, doi:10.5194/acp-11-4645-2011.

Sander, S. P., et al. (2011), *Chemical Kinetics and Photochemical Data for Use in Atmospheric Studies Evaluation No. 17*, JPL Publ. 10-6, Jet Propulsion Lab., Calif. Inst. of Technol., Pasadena, Calif.

Semeniuk, K., V. I. Fomichev, J. C. McConnell, C. Fu, S. M. L. Melo, and I. G. Usoskin (2011), Middle atmosphere response to the solar cycle in irradiance and ionizing particle precipitation, *Atmos. Chem. Phys.*, *11*, 5045–5077, doi:10.5194/acp-11-5045-2011.

Seppälä, A., P. T. Verronen, M. A. Clilverd, C. E. Randall, J. Tamminen, V. F. Sofieva, L. Backman, and E. Kyrölä (2007), Arctic and Antarctic polar winter NO_x and energetic particle precipitation in 2002–2006, *Geophys. Res. Lett.*, *34*, L12810, doi:10.1029/2007GL029733.

Sinnhuber, M., H. Nieder, and N. Wieters (2012), Energetic particle precipitation and the chemistry of the mesosphere/lower thermosphere, *Surv. Geophys.*, *33*, 1281–1334, doi:10.1007/s10712-012-9201-3.

Smith, A. K., M. López-Puertas, M. García-Comas, and S. Tukiainen (2009), SABER observations of mesospheric ozone during NH late winter 2002–2009, *Geophys. Res. Lett.*, *36*, L23804, doi:10.1029/2009GL040942.

Verronen, P. T., and R. Lehmann (2013), Analysis and parameterisation of ionic reactions affecting middle atmospheric HO_x and NO_y during solar proton events, *Ann. Geophys.*, *31*, 909–956, doi:10.5194/angeo-31-909-2013.

Verronen, P. T., A. Seppälä, M. A. Clilverd, C. J. Rodger, E. Kyrölä, C.-F. Enell, T. Ulich, and E. Turunen (2005), Diurnal variation of ozone depletion during the October–November 2003 solar proton events, *J. Geophys. Res.*, *110*, A09S32, doi:10.1029/2004JA010932.

Verronen, P. T., A. Seppälä, E. Kyrölä, J. Tamminen, H. M. Pickett, and E. Turunen (2006), Production of odd hydrogen in the mesosphere during the January 2005 solar proton event, *Geophys. Res. Lett.*, *33*, L24811, doi:10.1029/2006GL028115.